Molecular Therapy
Nucleic Acids
Original Article

Gold Nanoparticles for *BCR-ABL1* Gene Silencing: Improving Tyrosine Kinase Inhibitor Efficacy in Chronic Myeloid Leukemia

Raquel Vinhas,[1] Alexandra R. Fernandes,[1] and Pedro V. Baptista[1]

[1]UCIBIO, Departamento de Ciências da Vida, Faculdade de Ciências e Tecnologia, Universidade Nova de Lisboa, Campus da Caparica, 2829-516 Caparica, Portugal

Introduction of tyrosine kinase inhibitors for chronic myeloid leukemia treatment is associated with a 63% probability of maintaining a complete cytogenetic response, meaning that over 30% patients require an alternative methodology to overcome resistance, tolerance, or side effects. Considering the potential of nanotechnology in cancer treatment and the benefits of a combined therapy with imatinib, a nanoconjugate was designed to achieve *BCR-ABL1* gene silencing. Gold nanoparticles were functionalized with a single-stranded DNA oligonucleotide that selectively targets the e14a2 *BCR-ABL1* transcript expressed by K562 cells. This gold (Au)-nanoconjugate showed great efficacy in gene silencing that induced a significant increase in cell death. Variation of BCL-2 and BAX protein expression, an increase of caspase-3 activity, and apoptotic bodies in cells treated with the nanoconjugate demonstrate its aptitude for inducing apoptosis on K562 BCR-ABL1-expressing cells. Moreover, the combination of the silencing Au-nanoconjugate with imatinib prompted a decrease of imatinib IC_{50}. This Au-nanoconjugate was also capable of inducing the loss of viability of imatinib-resistant K562 cells. This strategy shows that combination of Au-nanoconjugate and imatinib make K562 cells more vulnerable to chemotherapy and that the Au-nanoconjugate alone may overcome imatinib-resistance mechanisms, thus providing an effective treatment for chronic myeloid leukemia patients who exhibit drug tolerance.

INTRODUCTION

Chronic myeloid leukemia (CML) affects approximately 1.5 million people worldwide and is characterized by the uncontrolled proliferation of myeloid cells in the bone marrow and blood.[1] The disease hallmark results from a genetic abnormality: a reciprocal chromosomal translocation between the long arms of chromosomes 9 and 22, designated as t(9;22)(q34;q11), creating a derivative 9q+ and a shortened 22q−, the Philadelphia (Ph) chromosome. Due to different possible breakpoints on chromosome 22 and alternative splicing events, several transcripts can originate from this translocation.[2–4] However, the e14a2 and e13a2 are present in most CML patients, with the e14a2 transcript representing 55% of Ph+ cases.[5] CML was the first malignancy in which a unique chromosomal abnormality was identified in more than 90% of the cases.[1,6]

All *BCR-ABL1* gene fusions described thus far encode for a constitutively active tyrosine kinase that plays a central role on leukemogenesis, since it disturbs downstream signaling pathways, causing enhanced proliferation, differentiation arrest, and resistance to cell death.[7] Hence, targeted tyrosine kinase inhibitors (TKIs) are the standard treatment for CML, which works best on early stages of the disease, with imatinib (IM) being the first-line treatment. Based on the Sokal risk score at the time of diagnosis for patient age, drug cost, comorbidities, drug toxicity, and gene mutation profile, other TKIs can be administered: dasatinib, nilotinib, bosutinib, or ponatinib.[4] Although more effective than IM, these TKIs are associated with different safety profiles, and their impact on long-term overall survival remains undetermined.[8] Despite the efficacy of TKI treatment, early relapse and TKI resistance, which have been associated with BCR/ABL1-dependent or -independent mechanisms, are still major concerns.[9–11]

Antisense DNA therapy is a powerful instrument for regulating the expression of genes associated with disease, with the potential to be used as an adjuvant to conventional chemotherapy.[12,13] Single-stranded DNA (ssDNA) oligonucleotides may be delivered into cells and target specific mRNA molecules, inhibiting expression of the encoded protein.[14] Gold nanoparticles (AuNPs) protect the antisense oligonucleotide against degradation by RNases, thus increasing circulation half-life and, therefore, the payload of therapeutic agent that is delivered to cells. The potential of AuNPs to vectorize actuators for gene silencing via simple assembly onto the nanoparticle core has been demonstrated in vitro and in vivo for a range of different nucleic acid moieties, including small interfering RNA (siRNA)[15–19] and antisense ssDNA.[20–24] The latter has been proven to be very specific, particularly when using stem-looped oligonucleotides, making it

Received 2 February 2017; accepted 3 May 2017;
http://dx.doi.org/10.1016/j.omtn.2017.05.003.

Correspondence: Pedro V. Baptista, UCIBIO, Departamento de Ciências da Vida, Faculdade de Ciências e Tecnologia, Universidade Nova de Lisboa, Campus da Caparica, 2829-516 Caparica, Portugal.
E-mail: pmvb@fct.unl.pt
Correspondence: Alexandra R. Fernandes, UCIBIO, Departamento de Ciências da Vida, Faculdade de Ciências e Tecnologia, Universidade Nova de Lisboa, Campus da Caparica, 2829-516 Caparica, Portugal.
E-mail: ma.fernandes@fct.unl.pt

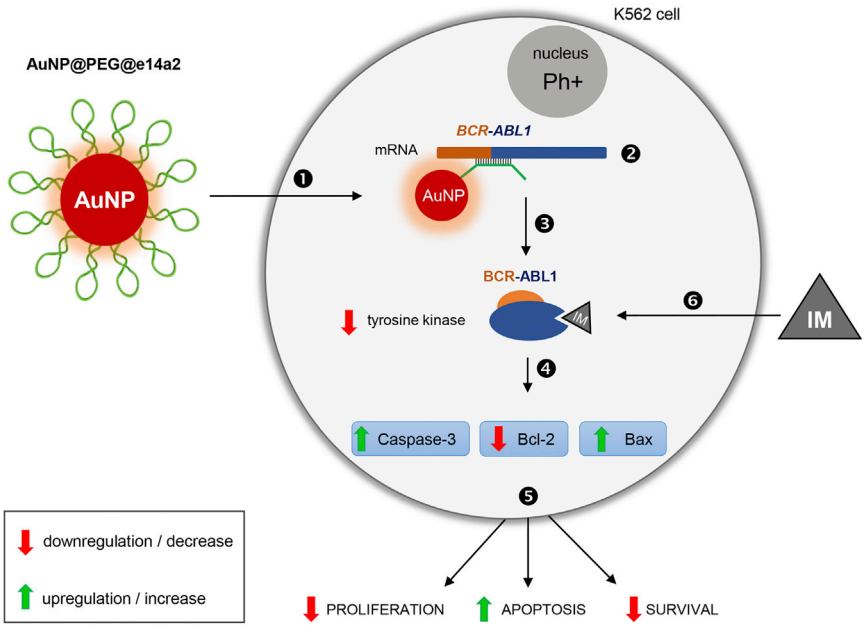

Figure 1. Gold-Nanoparticle-Based BCR-ABL Gene Silencing

(1–6) In (1), gold nanoparticles (AuNPs functionalized with the e14a2 antisense hairpin ssDNA oligonucleotide (AuNP@PEG@e14a2) are internalized by K562 cells, a CML in vitro model. (2) The Au-nanoconjugate recognizes *BCR-ABL1* mRNA expressed by these cells. The hairpin opens in the presence of the complementary *BCR-ABL1* sequence, silencing gene expression and triggering mRNA degradation and (3) leading to the translation inhibition of the encoded tyrosine kinase and to (4) the downregulation of BCL2 and the upregulation of BAX and caspase-3 activity. (5) The apoptotic pathway increases CML cell apoptosis and decreases proliferation and survival, ultimately killing BCR-ABL1 leukemic cells. (6) Conjugation of tyrosine kinase inhibitors (IM) with the gene-silencing Au-nanoconjugate should be an effective way to overcome chemotherapy resistance.

suitable for the real-time monitoring of gene silencing via gold nanobeacons.[20–22]

In this study, we silenced the *BCR-ABL1* chimeric gene in vitro, using AuNPs functionalized with an antisense oligonucleotide (see Figure 1). The effects of the construct on BCR-ABL1 signaling pathways were further assessed through the evaluation of the changes in the expression levels of key players of cell proliferation and apoptosis/survival. Besides gene silencing evaluation, a combined therapy assay was performed to understand the role of the gold (Au)-nanoconjugate as an adjuvant to the conventional treatment for CML (IM), even in K562 cells resistant to IM. The effect of this Au-nanoconjugate may be crucial in overcoming toxicity and resistance mechanisms related to TKI administration.

RESULTS AND DISCUSSION

Standard chemotherapy may be combined with gene silencing approaches to assist cancer cell death, where silencing oligonucleotides recognize a specific gene product to shut down the production of a protein associated to disease. This way, those cells harboring the selected gene marker will be selectively targeted for enhanced destruction, allowing for improvement of efficacy. In CML, the molecular hallmark of disease—*BCR-ABL1* fusion transcript—may be used to selectively target malignant cells in combination with a particular TKI, thus potentiating cell death. Gene silencing has profited from nanovectorization strategies that extend circulation half-life of therapeutic nucleic acids while improving cell uptake.[25,26] Here, we used AuNPs to deliver a specific oligo targeting the *BCR-ABL1* mRNA sequence in CML cells, where the silencing moiety was in a stem-loop configuration to improve selectivity and specificity toward target sequence.[22,27] AuNPs with 14 nm in diameter were synthesized and further functionalized with polyethylene glycol (AuNP@PEG) and with a ssDNA targeting the *BCR-ABL1* mRNA sequence (50 oligonucleotide density per nanoparticle). The nanoconjugates were characterized by UV-visible (UV-Vis) spectroscopy, transmission electron microscopy (TEM) and dynamic light scattering (DLS) (Supplemental Information; Table S1). Data show nanoconjugates with a mean diameter of 51 nm (Supplemental Information; Table S1). Polyethylene glycol (PEG) functionalization is crucial to increase nanoconjugate solubility both in vivo and in vitro, reduce their uptake by the reticuloendothelial system, thus increasing AuNPs circulation time, and decrease serum and tissue protein association.[28]

BCR-ABL1 Gene Silencing and Cell Fate

Real-time qPCR analysis of *BCR-ABL1* gene expression shows that, after 12 hr of exposure of K562 cells to 0.6 nM silencing nanoconjugates, expression of the fusion transcript decreases till it reaches a minimum at 24 hr (Figure 2). After 72 hr, *BCR-ABL1* expression is completely restored, possibly due to oligonucleotide degradation and/or cell expansion over time, which increases the number of cells per nanoparticle applied in cell medium, but in line with what has been previously observed for other targets.[26,29] Together, these data show efficient gene silencing by the designed nanoconjugates.

Once effective gene silencing of *BCR-ABL1* was achieved, we investigated downstream control points for apoptosis/survival. A comparable transient effect was observed for *BCL2*, a downstream target gene of *BCR-ABL1*, which followed a similar reduction profile (Figure 2). This result further corroborates the overall cell effect of silencing *BCR-ABL1*, since BCL2 expression levels are strongly regulated by BCR-ABL1 in cancer cells. In fact, in the signaling pathway that ultimately culminates in increased survival and unregulated proliferation of Ph+ cells, *BCR-ABL1* prevents apoptosis by inducing BCL2 through a cascade of responses involving constitutive RAS activation and *BCL2* gene regulation.[30] Flow cytometry data also corroborate

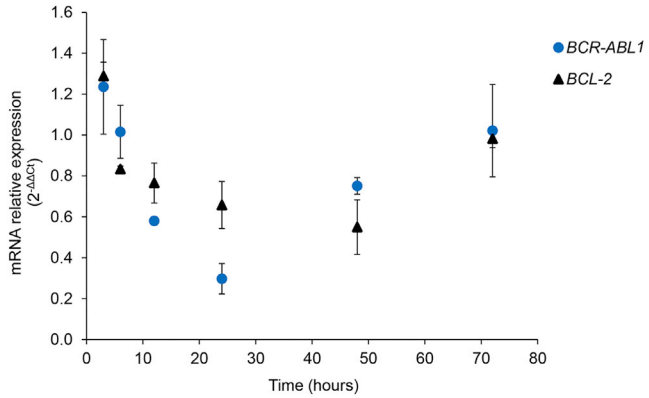

Figure 2. Au-Nanoconjugates Effectively Silence *BCR-ABL1*

BCR-ABL1 (blue full circle) and *BCL2* (black full triangle) mRNA relative expression after treatment of K562 cells with AuNP@PEG and AuNP@PEG@e14a2. Data were normalized to the *18S* gene and then to cells exposed to AuNP@PEG. Ct, threshold cycle. Error bars represent the SEM of at least three independent experiments.

these trends for K562 cells treated with the Au-nanoconjugate (see Supplemental Information; Figure S1). Measurement of side scatter intensity (SSC) in flow cytometry is an efficient way to study cell interaction with AuNPs associated with their strong scattering.[31] SSC values increased for cells treated with the Au-nanoconjugate, peaking at 24 hr (see Supplemental Information; Figure S1).

In CML, *BCR-ABL1* induces the deregulation of cell proliferation with the inhibition of apoptosis and an increased survival rate. Exposure of K562 cells to the Au-nanoconjugate significantly delayed cell growth, particularly for the 24- to 48-hr period (Figure 3A). In that period, cell-doubling time was circa 116 hr, which is much slower than control (PBS) or control vehicle (AuNP@PEG): 17 hr and 20 hr, respectively. These data are in accordance with gene expression studies discussed earlier, where the window of silencing effectiveness was between 24 hr and 48 hr. Cell-viability studies by the MTS assay also show a decrease of cell viability of 25% at 48 hr (Figure 3B). The short-term effect induced by the construct might be associated with the increase in cell numbers after 48 hr, skewing the most efficient cell:Au-nanoconjugate ratio. The Au-nanoconjugate functionalized with a scrambled oligonucleotide showed no effect on cell viability. As such, the previously observed reduction in cell viability (25%; Figure 3B) was due to the oligonucleotide effect by targeting the fusion e14a2 *BCR-ABL1* transcript.

The Au-nanoconjugate specificity toward cells expressing the e14a2 *BCR-ABL1* transcript was confirmed by assessing cell viability on THP1 (*BCR-ABL1*-negative cell line derived from an acute monocytic leukemia patient) and BV173 (CML cell line derived from an e13a2-positive patient). The silencing nanoconjugate, specific for the e14a2 *BCR-ABL1* isoform, solely promoted cell-viability reduction on K562 cells, indicating that the construct is highly specific, since the e14a2 and e13a2 transcripts share the *ABL1* part of the sequence (Figure 3C). This high-sequence specificity had been previously demonstrated for in vitro CML diagnostics in clinical samples using AuNPs.[32] Because the sequence only targets the isoform of interest, it acts as a molecular marker for targeted therapy. As expected, IM had no effect on THP1 but decreased cell viability on BV173 and K562, since it was designed to bind specifically to the active site of BCR-ABL1 proteins.[33]

The IM mechanism of action involves blocking the cell-surface receptor that subsequently induces cancer cell death via apoptosis.[33,34] We investigated the triggering of apoptotic pathways by cells challenged with our silencing nanoconjugate, AuNP@PEG@e14a2. Cell nuclei undergo several morphological changes even at early apoptosis, including chromatin condensation, nuclear fragmentation, and the presence of apoptotic bodies, which can be visualized using a fluorescent DNA dye (Hoechst) (Figure 4).[35] The silencing nanoconjugates were shown to induce an increase on the number of apoptotic cells at 48 hr, when compared to normal cells, cells exposed to AuNP@PEG@scramble, or cells exposed to AuNP@PEG, which does not induce apoptosis (see Supplemental Information; Figure S2).

The anti-apoptotic protein BCL2 and pro-apoptotic protein BAX are important regulators in the mitochondrial apoptotic pathway, particularly in *BCR-ABL1*-expressing cells. Inhibition of apoptosis is thought to result from activation of the phosphoinositide 3-kinase and RAS pathways, with induction through AKT of *c-MYC* and *BCL2*, and variation of their expression levels is of great importance for regulating apoptosis.[36] Many chemotherapeutic agents, including TKIs, trigger apoptotic cell death by activating caspases. Upon an apoptotic stimulus, initiator caspases (e.g., caspase-8 and caspase-9) cleave and activate executioner caspases (e.g., caspase-3), inducing proteolytic cleavage of specific apoptotic substrates that culminate in cell death.[37] In fact, the observed pro-apoptotic effect of our silencing nanoconjugate corroborated data attained from the gene silencing experiments (Figure 2), where *BCL2* gene expression was downregulated. To further confirm the downstream events triggered by direct silencing of *BCR-ABL1* that ultimately induce apoptosis, we evaluated the actual expression of these two canonical apoptotic pathways: the BCL2/BAX and caspase activation (Figure 5).

Silencing of *BCR-ABL1* using AuNP@PEG@e14a2 not only downregulated BCL2 but also upregulated BAX expression, shifting K562 cells from the anti-apoptotic setting characteristic of BCR-ABL1-expressing cells to pro-apoptotic (Figures 5A and 5B). A 2-fold change on the BAX/BCL2 ratio was obtained for AuNP@PEG@e14a2, higher than that of IM, the gold standard of CML chemotherapeutics (Figure 5C). Caspase-3 activity was then measured at 24 and 48 hr and, although no effect was observed at the shorter time point, there was an increase in caspase-3 activity at 48 hr, mimicking the effect induced by IM (Figure 5D). The time-dependent profile observed with this assay also highlights the delay observed between gene silencing (higher effect at 24 hr) and protein expression/activation (higher effect at 48 hr).

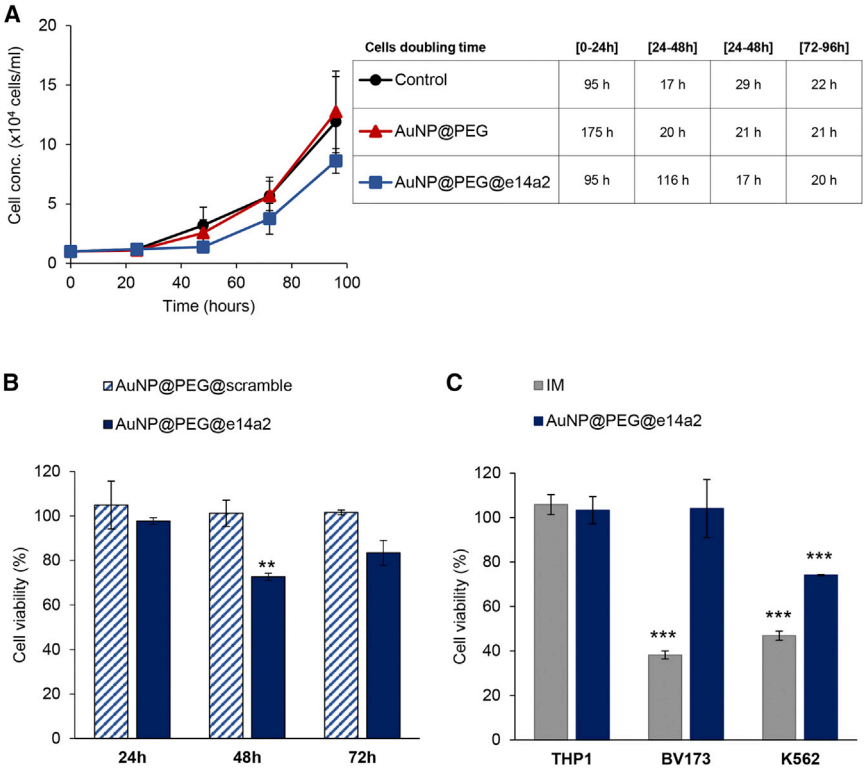

Figure 3. . Cell Proliferation Assays upon Exposure to the Au-Nanoconjugate

(A) Cell viability count via trypan blue exclusion assay on untreated K562 cells (black circles), cells exposed to AuNP@PEG (red triangles), and silencing nanoconjugate (blue squares). Cells' doubling time was also calculated (embedded table). conc., concentration. (B) Cell viability over time on K562 cells challenged with AuNP@PEG@e14a2 (silencing nanoconjugate) and AuNP@PEG@scramble. (C) Sequence specificity of AuNP@PEG@e14a2 toward *BCR-ABL1* measured by impact on cell viability on THP1, BV173, and K562 cells; cells were also challenged with 0.1 μM IM, which is specific for *BCR-ABL1*. Data on plots (B) and (C) were normalized to AuNP@PEG. **p < 0.01; ***p < 0.001, Tukey's test statistical significance versus first column.

Improving CML Cell Death by a Combination of IM and Silencing Nanoconjugates

Recently, the use of combinatory strategies for effective therapy has been the focus of numerous studies to overcome the consequences of TKI resistance and long-term treatments in CML. In fact, TKI resistance affects nearly 30% of CML patients and is related to the overexpression of *BCR-ABL1*, mutational events, drug metabolism, transport and intracellular influx, and patient non-compliance.[8]

The efficacy of the Au-nanoconjugate as an adjuvant to conventional therapy was assessed by measuring cell viability after a combined 48-hr challenge with the silencing nanoconjugate and increasing concentrations of IM (0.01–10 μM). AuNP@PEG@e14a2 combined with IM increased efficacy by 23% when compared to IM alone, demonstrating the ability of the nanoconjugate to enhance the effect of IM on cell proliferation. It should be mentioned that challenging cells with AuNP@PEG seem to slightly increase cell viability, but even so, when compared to IM+AuNP@PEG, the combinatory approach of IM + silencing nanoconjugate was 30% more effective (Table 1).

The effect of the Au-nanoconjugate on IM-resistant cells was also analyzed (Figure 6). IM-resistant K562 cells do not respond to the concentration of IM corresponding to the half maximal inhibitory concentration (IC_{50}) of sensitive parental K562 cells (as shown in Figure 3C) and is due to an increase of the *BCR-ABL1* expression rather than to mutations to *ABL1* (see Figure S3). Remarkably, AuNP@PEG@e14a2 induced a significant reduction (30%) of viability in K562-IM-resistant cells (Figure 6).

Conclusions

Here, we show that using a sequence-selective silencing nanoconjugate, AuNP@PEG@e14a2, may be used to regulate CML cell proliferation and apoptosis (see Figure 1). Such silencing potential is exerted with great sequence selectivity that may be used to selectively target those cells harboring a particular gene/gene isoform. This strategy may provide an additional wave of destruction to current TKIs, particularly in patients that display TKI toxicity and/or resistance and frequently relapse. This strategy is clearly aligned with the recent recommendations of the European LeukemiaNet,[38] due to the high cost to CML patients and public institutions of long-term treatment and the occurrence of adverse effects.[39] Our strategy might open the way for the development of specific and selective molecular targeting approaches that should impact how we perceive chemotherapy and provide for enhanced precision for a range of drugs that have already proven their tremendous efficacy in the clinics.

MATERIALS AND METHODS

Au-Nanoconjugate Synthesis and Characterization

AuNPs of 14 nm were synthesized by the citrate reduction method.[40] AuNPs were first functionalized with PEG modified with a thiol group ($C_{15}H_{32}O_7S$, 356.48 Da) (AuNP@PEG), corresponding to 30% saturation of AuNPs' surface. AuNP@PEGs were subsequently functionalized with the thiolated oligonucleotide: 5′-TTTCGGC GCTGAAGGGCTTTTGAACTCCGAAA-3′ (palindromic sequence underlined; sequence targeting the fusion e14a2 *BCR-ABL1* transcript was derived from GenBank: AJ131466.1) (AuNP@PEG@e14a2-Au-nanoconjugate).[32] A palindromic sequence was added to allow the stem-loop structure. Au-nanoconjugates were prepared at a 1:100 (AuNP:oligonucleotide) ratio and centrifuged for 40 min at 14,000 × *g*, and the precipitate was washed three times with

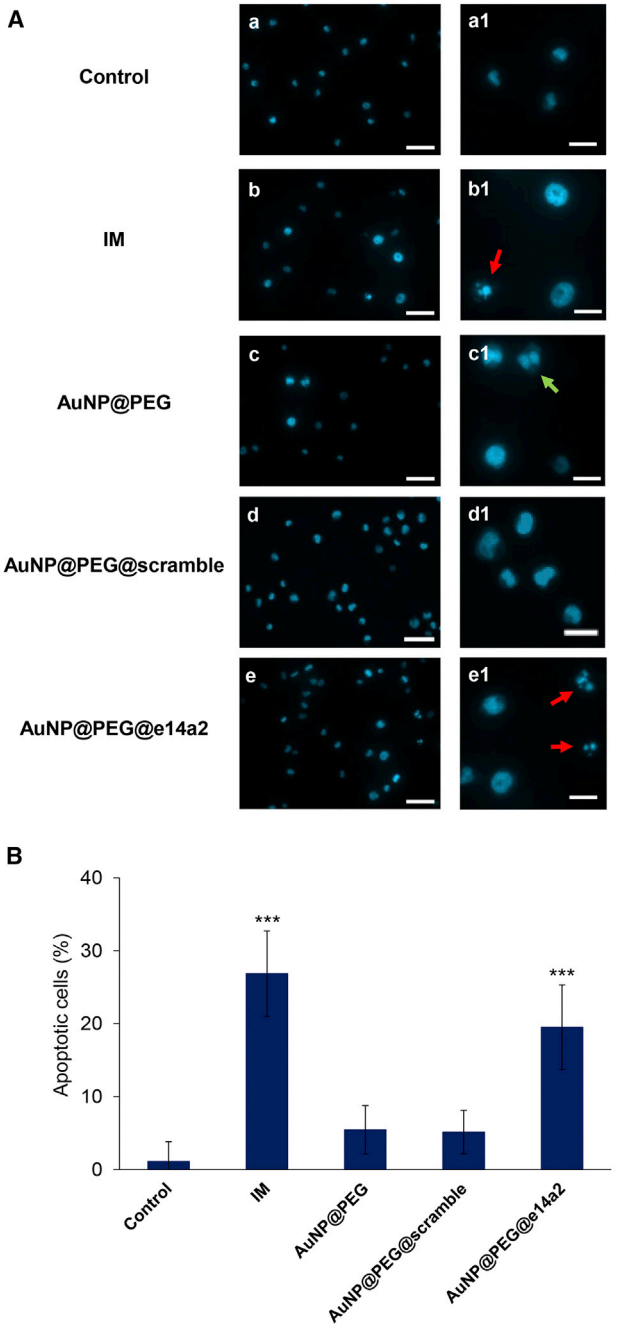

Figure 4. Silencing Nanoconjugates Induce Apoptosis

(A) Hoechst staining on non-treated (control) cells (a and a1) or cells treated for 48 hr with 0.1 μM IM (b and b1), 0.6 nM AuNP@PEG (c and c1), 0.7 nM AuNP@PEG@scramble (d and d1), or 0.6 nM Au-nanoconjugate (corresponding to 30 nM of oligonucleotide) (e and e1). Representative fluorescence microscopy images are shown in (a)–(d); scale bars, 50 μm. Zoomed images for each condition are shown at right, in (a1)–(d1) (scale bars, 20 μm), for better visualization between apoptotic (red arrows) or mitotic (green arrow) cell morphology. (B) Apoptotic events count based on nucleus morphology and formation of apoptotic bodies after Hoechst staining. ***$p < 0.001$, Tukey's test statistical significance when compared to control condition and AuNP@PEG.

diethylpyrocarbonate-treated water. The number of oligonucleotides bonded to the AuNP surface was determined in each supernatant using Quant-iT OliGreen ssDNA Reagent (ThermoFisher Scientific). The resulting Au-nanoconjugates were stored at 4°C in the dark and characterized by UV-Vis spectroscopy, TEM, and DLS.

A control scrambled oligonucleotide 5′-TTTCGGGTTGACGTTAG CCGGATCTACCGAAA-3′ was also prepared and characterized under the same conditions: AuNP@PEG@scramble.

Cell Culture and Au-Nanoconjugate Challenge

The immortalized cell line K562 (cell line positive for BCR-ABL1 e14a2 fusion transcript) derived from a CML patient in blast crisis (American Type Culture Collection [ATCC] reference no. CCL-243)[41] was cultured in DMEM supplemented with 10% fetal bovine serum (FBS) at 37°C with 5% CO_2 and 99% relative humidity.

For the assays, cells were seeded at a density of 1×10^5 cells per well (24-well plates) or 5×10^3 cells per well (96-well plates) and challenged with 0.6 nM Au-nanoconjugate, corresponding to 30 nM oligonucleotide (Au:oligonucleotide ratio = 1:50). As control, cells were exposed to 0.6 nM AuNP@PEG (control vehicle); to 0.7 nM AuNP@PEG@scramble (corresponding to 30 nM oligonucleotide; Au:oligonucleotide ratio = 1:44); or to 0.1 μM IM, and PBS as control for IM.

Sequence specificity was also tested using two different cell lines: an acute monocytic leukemia cell line (THP1; ATCC reference no. TIB-202)[41] negative for *BCR-ABL1* and a CML cell line (BV173; German Collection of Microorganisms and Cell Cultures [DSMZ] reference no. ACC 20)[42] positive for the BCR-ABL1 e13a2 transcript, cultured as described earlier. Incubation of cells with nanoconjugates or IM was performed at a density of 2.5×10^4 cells per well (96-well plate).

IM-resistant K562 cells were generated via incubation of K562-sensitive cells with increasing concentrations of IM (starting with a concentration of 0.01 μM up to 1 μM) for more the 50 passages (K562-IM). *BCR-ABL1* gene expression on K562-IM cells was evaluated via qPCR as described in the following section (Gene Expression Analysis). Data were analyzed by the comparative threshold cycle (Ct) method ($2^{-\Delta\Delta Ct}$), where relative gene expression is given by quantification of *BCR-ABL1* relative to the internal control gene (*18S*), normalized to the control condition (parental K562 cells). To assess *BCR-ABL1* mutational status on K562-IM cells, a nested-PCR amplification was performed using primers shown in Table S2. Outer PCR conditions included an initial denaturation at 95°C for 5 min; 30 cycles of 94°C for 30 s, 55°C for 30 s, and 72°C for 1 min; and a final extension step at 72°C for 10 min. Inner PCR included an initial denaturation at 95°C for 5 min; 30 cycles of 94°C for 15 s, 55°C for 30 s, and 72°C for 1 min; and a final extension step at 72°C for 10 min. PCR products were sequenced at STAB VIDA.

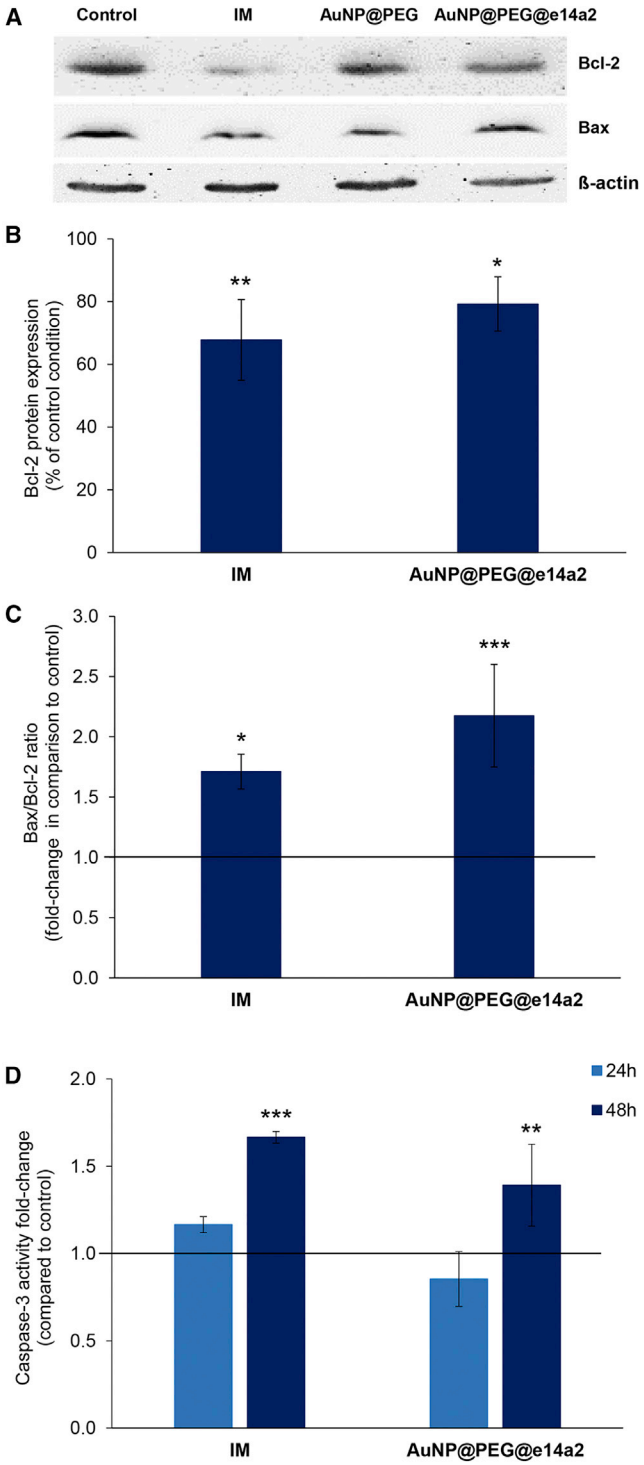

Figure 5. Triggering of Apoptotic Cascade via Combinatory Therapy

Expression of K562 cells BCL2 and BAX after exposure to the Au-nanoconjugate. (A) BCL2 (26 kDa) and BAX (21 kDa) protein quantification was performed via western blotting on cell extracts after a 48-hr exposure to 0.1 μM IM or 0.6 nM AuNP@PEG@e14a2. Band quantification was first normalized against β-actin (42 kDa) and, subsequently, to the control condition: cells without treatment or cells exposed to 0.6 nM AuNP@PEG. (B) BCL2 protein expression (control as 100%). (C) Apoptotic index of K562 cells, based on BAX/BCL2 ratio. (D) Caspase-3 activity on K562 cells after exposure to 0.1 μM IM or 0.6 nM AuNP@PEG@e14a2. Values were normalized against cells without treatment (value represented by the threshold). *$p < 0.05$; **$p < 0.01$; ***$p < 0.001$, Tukey's test statistical significance.

Gene Expression Analysis

Cells exposed to the different conditions (AuNP@PEG and Au-nanoconjugate) in 24-well plates were collected at different time points between 3 and 72 hr. Cells were centrifuged at 200 × *g* for 5 min at room temperature, and total RNA was extracted from cell pellets using TRIsure (Bioline) according to the manufacturer's instructions. Total RNA (100 ng) was reverse transcribed using the NZY M-MuLV First-Strand cDNA Synthesis kit (NZYTech).

qPCR amplification of cDNA was performed on a Corbett Rotor-Gene 6000 thermal cycler (QIAGEN) using the HOT FIREpol EvaGreen qPCR Mix (Solis BioDyne) with the following primers, at a concentration of 100 nM each: BCR forward (5′-GAAGTGTTTCAGAAGCT TCTCC-3′) and ABL1 reverse (5′-GTTTGGGCTTCACACCATT CC-3′); BCL2 forward (5′-CTTCGCCGAGATGTCCAGCCA-3′) and BCL2 reverse (5′-CGCTCTCCACACACATGACCC-3′); 18S forward (5′-GTAACCCGTTGAACCCCATT-3′) and 18S reverse (5′-CCATCCAATCGGTAGTAGCG-3′). qPCR conditions included an initial denaturation at 95°C for 15 min and 40 cycles of 95°C for 20 s, 55°C (BCR-ABL1 and 18S) or 65°C (BCL-2) for 20 s, and 72°C for 30 s. qPCR data were analyzed by the Ct method ($2^{-\Delta\Delta Ct}$), where relative gene expression is given by quantification of the gene of interest (*BCR-ABL1* or *BCL2*) relative to internal control gene (*18S*), normalized to the control condition (cells exposed to AuNP@PEG).[43]

Flow Cytometry

Cells were exposed to the Au-nanoconjugate in 24-well plates, recovered by centrifugation at 400 × *g* for 5 min at 4°C, and washed with cold PBS. Cells were resuspended in PBS and analyzed by measuring side scatter peak area (SSC-A) of 10,000 events per reading in an Attune Acoustic Focusing Cytometer (ThermoFisher Scientific).

Cell Proliferation Assays

K562 cells were plated in 24-well plates, and growth rate was determined by counting the number of viable cells after challenge with AuNP@PEG or AuNP@PEG@e14a2 nanoconjugates using the Trypan Blue (0.2%) Exclusion assay (ThermoFisher Scientific), where viable cells possess intact cell membranes that exclude the dye, whereas dead cells do not and appear blue.[44] Cell-doubling time was calculated as: (time × log(2))/(log(final concentration) − log(initial concentration)).

Additionally, K562, THP1, and BV173 cells exposed to IM, AuNP@PEG and Au-nanoconjugates were assessed in 96-well plates using the CellTiter 96 AQ_{ueous} Non-Radioactive Cell Proliferation Assay (MTS, Promega).[45] Absorbance at 490 nm was measured in a

Table 1. Effect on IM when Combined with Silencing Nanoconjugates

	IM	IM + AuNP@PEG	IM + AuNP@PEG@e14a2
IC_{50} of IM (in μM)	0.22	0.24	0.17***

IC_{50} values were calculated for 48 hr. ***p < 0.001, Bonferroni's test statistical significance, compared to IM or IM+AuNP@PEG.

Microplate Reader Infinite M200 (Tecan), and values were corrected to the respective control conditions (without cells). The IC_{50} for IM at 48 hr was also determined via MTS assay by exposing K562 cells to growing IM concentrations ranging from 0.01 to 10 μM.

Apoptosis Assay

K562 cells cultured in a 24-well plate were fixed with 4% paraformaldehyde, washed with PBS, and stained using 10 μg/mL Hoechst 33258 (ThermoFisher Scientific).[46,47] At least six images per condition were collected using an AxioImager D2 fluorescence microscope (Carl Zeiss) with a 100× immersion objective, a 365-nm excitation filter, and a 445/50-nm emission filter (filter set 49, Carl Zeiss).

Western Blot

Cells were washed with PBS and resuspended in lysis buffer [150 mM NaCl, 50 mM Tris (pH 8.0), 5 mM EDTA, 2% (v/v) NP-40, 1× phosphatase inhibitor (PhosStop, Roche), 1× protease inhibitor (cOmplete Mini, Roche), 1 mM PMSF, and 0.1% (w/v) DTT]. Whole-cell extracts were sonicated and centrifuged at 5000 × *g* for 10 min. The supernatant was recovered, and protein concentration was determined using the Pierce 660nm Protein Assay Reagent (ThermoFisher Scientific) per manufacturer's specifications. Then, 25 μg total protein extracts were separated by SDS-PAGE in a 10% (37.5:1) acrylamide-bisacrylamide gel (Merck Millipore). Following electrophoretic transfer onto a 0.45-μm nitrocellulose membrane (GE Healthcare) and blocking with 5% (w/v) milk solution in Tris-buffered saline with 0.1% (v/v) Tween 20 (TBST), blots were incubated per manufacturer's instructions for 1 hr at room temperature with primary antibodies against BCL2 (reference no. B3170, Sigma), BAX (reference no. 32503, Abcam), and β-actin (reference no. A5441, Sigma). Membranes were washed with TBST and incubated with the appropriate secondary antibody conjugated with horseradish peroxidase (reference no. 7074 or 7076, Cell Signaling Technology). WesternBright ECL (Advansta) was applied to the membranes, and signal was acquired in a Gel Doc imager (Bio-Rad).

Caspase-3 Activity

Caspase-3 activity was assessed using the Caspase-3 Apoptosis Detection Kit from Santa Cruz Biotechnology, as described by Luis et al.[48] Briefly, 50 μL cell lysates were diluted in 200 μL reaction buffer containing 10 mM DTT and 5 μL fluorometric substrate DEVD-AFC (7-amino-4-trifluoromethyl coumarin) and incubated at 37°C for 1 hr. Caspase-3 activity was quantified by fluorescent detection of free AFC after cleavage from DEVD peptide. The free AFC level was measured using a Varian Cary Eclipse Fluorescence Spectrophotometer (Agilent Technologies) with a 400-nm excitation filter and a 505-nm emission filter.

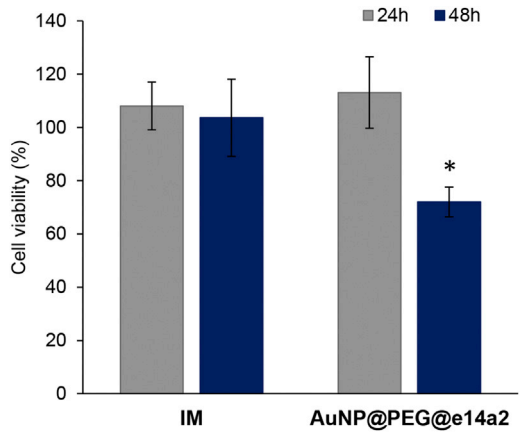

Figure 6. . Viability via MTS Assay of K562 Cells Resistant to IM
Cells were challenged with 0.1 μM IM or 0.6 nM AuNP@PEG@e14a2 for 24 or 48 hr. *p < 0.05, Bonferroni's test statistical significance, compared to the control condition AuNP@PEG.

Statistical Analysis

All data are expressed as mean ± SE from at least three independent experiments. Statistical significance was evaluated through one-way ANOVA followed by Tukey's multiple comparison test. Mean differences between groups were determined with a 95% confidence interval. Statistical significance of data from Table 1 and Figure 6 was evaluated through two-way ANOVA followed by Bonferroni's test.

SUPPLEMENTAL INFORMATION

Supplemental Information includes Supplemental Experimental Procedures, three figures, and two tables and can be found with this article online at http://dx.doi.org/10.1016/j.omtn.2017.05.003.

AUTHOR CONTRIBUTIONS

A.R.F. and P.V.B. designed the study. R.V. performed the experiments. All authors were involved in data analysis and drafting of the manuscript.

CONFLICTS OF INTEREST

The authors declare no conflict of interest related to this manuscript.

ACKNOWLEDGMENTS

This work was supported by FCT/MEC to Unidade de Ciências Biomoleculares Aplicadas – UCIBIO by national funds (UID/Multi/04378/2013) and co-financed by the ERDF under the PT2020 Partnership Agreement (POCI-01-0145-FEDER-007728). R.V. acknowledges FCT/MEC for PD/BD/52211/2013. We also acknowledge P. Martins, C. Roma-Rodrigues, and B. Oliveira for the induction and characterization of IM-resistant K562 cells.

REFERENCES

1. Jabbour, E., and Kantarjian, H. (2016). Chronic myeloid leukemia: 2016 update on diagnosis, therapy, and monitoring. Am. J. Hematol. *91*, 252–265.
2. Melo, J.V. (1996). The diversity of BCR-ABL fusion proteins and their relationship to leukemia phenotype. Blood *88*, 2375–2384.
3. Torres, F., Ivanova-Dragoeva, A., Pereira, M., Veiga, J., Rodrigues, A.S., Sousa, A.B., Tavares, P., and Fernandes, A.R. (2007). An e6a2 BCR-ABL fusion transcript in a CML patient having an iliac chloroma at initial presentation. Leuk. Lymphoma *48*, 1034–1037.
4. Vinhas, R., Cordeiro, M., Pedrosa, P., Fernandes, A.R., and Baptista, P.V. (2017). Current trends in molecular diagnostics of chronic myeloid leukemia. Leuk. Lymphoma *58*, 1791–1804.
5. Hanfstein, B., Lauseker, M., Hehlmann, R., Saussele, S., Erben, P., Dietz, C., Fabarius, A., Proetel, U., Schnittger, S., Haferlach, C., et al.; SAKK and the German CML Study Group (2014). Distinct characteristics of e13a2 versus e14a2 BCR-ABL1 driven chronic myeloid leukemia under first-line therapy with imatinib. Haematologica *99*, 1441–1447.
6. Rowley, J.D. (1973). Letter: a new consistent chromosomal abnormality in chronic myelogenous leukaemia identified by quinacrine fluorescence and Giemsa staining. Nature *243*, 290–293.
7. Quintás-Cardama, A., and Cortes, J. (2009). Molecular biology of bcr-abl1-positive chronic myeloid leukemia. Blood *113*, 1619–1630.
8. Rosti, G., Castagnetti, F., Gugliotta, G., and Baccarani, M. (2017). Tyrosine kinase inhibitors in chronic myeloid leukaemia: which, when, for whom? Nat. Rev. Clin. Oncol. *14*, 141–154.
9. Mahon, F.X. (2012). Is going for cure in chronic myeloid leukemia possible and justifiable? Hematology Am. Soc. Hematol. Educ. Program *2012*, 122–128.
10. Carella, A.M., Branford, S., Deininger, M., Mahon, F.X., Saglio, G., Eiring, A., Khorashad, J., O'Hare, T., and Goldman, J.M. (2013). What challenges remain in chronic myeloid leukemia research? Haematologica *98*, 1168–1172.
11. Helgason, G.V., Mukhopadhyay, A., Karvela, M., Salomoni, P., Calabretta, B., and Holyoake, T.L. (2013). Autophagy in chronic myeloid leukaemia: stem cell survival and implication in therapy. Curr. Cancer Drug Targets *13*, 724–734.
12. Szczylik, C., Skorski, T., Nicolaides, N.C., Manzella, L., Malaguarnera, L., Venturelli, D., Gewirtz, A.M., and Calabretta, B. (1991). Selective inhibition of leukemia cell proliferation by BCR-ABL antisense oligodeoxynucleotides. Science *253*, 562–565.
13. Moreno, P.M., and Pêgo, A.P. (2014). Therapeutic antisense oligonucleotides against cancer: hurdling to the clinic. Front Chem. *2*, 87.
14. Watts, J.K., and Corey, D.R. (2012). Gene silencing by siRNAs and antisense oligonucleotides in the laboratory and the clinic. J. Pathol. *226*, 365–379.
15. Conde, J., Ambrosone, A., Sanz, V., Hernandez, Y., Marchesano, V., Tian, F., Child, H., Berry, C.C., Ibarra, M.R., Baptista, P.V., et al. (2012). Design of multifunctional gold nanoparticles for in vitro and in vivo gene silencing. ACS Nano. *6*, 8316–8324.
16. Wu, J., Liu, B., Wu, H., Wu, Y., Zhang, W., Zhao, S., Zhang, L., Pan, X., Gao, W., Wang, X., et al. (2016). A gold nanoparticle platform for the delivery of functional TGF-β1 siRNA into cancer cells. J. Biomed. Nanotechnol. *12*, 800–810.
17. Lee, S.K., and Tung, C.H. (2016). siRNA nanoparticles for ultra-long gene silencing in vivo. Methods Mol. Biol. *1372*, 113–120.
18. Heinemann, D., Schomaker, M., Kalies, S., Schieck, M., Carlson, R., Murua Escobar, H., Ripken, T., Meyer, H., and Heisterkamp, A. (2013). Gold nanoparticle mediated laser transfection for efficient siRNA mediated gene knock down. PLoS ONE *8*, e58604.
19. Lee, S.K., Han, M.S., Asokan, S., and Tung, C.H. (2011). Effective gene silencing by multilayered siRNA-coated gold nanoparticles. Small *7*, 364–370.
20. Conde, J., Rosa, J., de la Fuente, J.M., and Baptista, P.V. (2013). Gold-nanobeacons for simultaneous gene specific silencing and intracellular tracking of the silencing events. Biomaterials *34*, 2516–2523.
21. Conde, J., Larguinho, M., Cordeiro, A., Raposo, L.R., Costa, P.M., Santos, S., Diniz, M.S., Fernandes, A.R., and Baptista, P.V. (2014). Gold-nanobeacons for gene therapy: evaluation of genotoxicity, cell toxicity and proteome profiling analysis. Nanotoxicology *8*, 521–532.
22. Cordeiro, M., Carvalho, L., Silva, J., Saúde, L., Fernandes, A.R., and Baptista, P.V. (2017). Gold nanobeacons for tracking gene silencing in Zebrafish. Nanomaterials (Basel) *7*, 10.
23. Huschka, R., Barhoumi, A., Liu, Q., Roth, J.A., Ji, L., and Halas, N.J. (2012). Gene silencing by gold nanoshell-mediated delivery and laser-triggered release of antisense oligonucleotide and siRNA. ACS Nano. *6*, 7681–7691.
24. Jiwaji, M., Sandison, M.E., Reboud, J., Stevenson, R., Daly, R., Barkess, G., Faulds, K., Kolch, W., Graham, D., Girolami, M.A., et al. (2014). Quantification of functionalised gold nanoparticle-targeted knockdown of gene expression in HeLa cells. PLoS ONE *9*, e99458.
25. Vigderman, L., and Zubarev, E.R. (2013). Therapeutic platforms based on gold nanoparticles and their covalent conjugates with drug molecules. Adv. Drug Deliv. Rev. *65*, 663–676.
26. Ding, Y., Jiang, Z., Saha, K., Kim, C.S., Kim, S.T., Landis, R.F., and Rotello, V.M. (2014). Gold nanoparticles for nucleic acid delivery. Mol. Ther. *22*, 1075–1083.
27. Kuang, T., Chang, L., Peng, X., Hu, X., and Gallego-Perez, D. (2017). Molecular beacon nano-sensors for probing living cancer cells. Trends Biotechnol. *35*, 347–359.
28. Jokerst, J.V., Lobovkina, T., Zare, R.N., and Gambhir, S.S. (2011). Nanoparticle PEGylation for imaging and therapy. Nanomedicine (Lond.) *6*, 715–728.
29. Chen, J., and Xie, J. (2012). Progress on RNAi-based molecular medicines. Int. J. Nanomedicine *7*, 3971–3980.
30. Sánchez-García, I., and Martín-Zanca, D. (1997). Regulation of Bcl-2 gene expression by BCR-ABL is mediated by Ras. J. Mol. Biol. *267*, 225–228.
31. Paino, I.M.M., Marangoni, V.S., de Oliveira, Rde.C., Antunes, L.M.G., and Zucolotto, V. (2012). Cyto and genotoxicity of gold nanoparticles in human hepatocellular carcinoma and peripheral blood mononuclear cells. Toxicol. Lett. *215*, 119–125.
32. Vinhas, R., Correia, C., Ribeiro, P., Lourenço, A., Botelho de Sousa, A., Fernandes, A.R., and Baptista, P.V. (2016). Colorimetric assessment of BCR-ABL1 transcripts in clinical samples via gold nanoprobes. Anal. Bioanal. Chem. *408*, 5277–5284.
33. Druker, B.J. (2008). Translation of the Philadelphia chromosome into therapy for CML. Blood *112*, 4808–4817.
34. Drullion, C., Trégoat, C., Lagarde, V., Tan, S., Gioia, R., Priault, M., Djavaheri-Mergny, M., Brisson, A., Auberger, P., Mahon, F.X., and Pasquet, J.M. (2012). Apoptosis and autophagy have opposite roles on imatinib-induced K562 leukemia cell senescence. Cell Death Dis. *3*, e373.
35. Elmore, S. (2007). Apoptosis: a review of programmed cell death. Toxicol. Pathol. *35*, 495–516.
36. Hata, A.N., Engelman, J.A., and Faber, A.C. (2015). The BCL-2 family: key mediators of the apoptotic response to targeted anticancer therapeutics. Cancer Discov. *5*, 475–487.
37. Kurokawa, M., Ito, T., Yang, C.S., Zhao, C., Macintyre, A.N., Rizzieri, D.A., Rathmell, J.C., Deininger, M.W., Reya, T., and Kornbluth, S. (2013). Engineering a BCR-ABL-activated caspase for the selective elimination of leukemic cells. Proc. Natl. Acad. Sci. USA *110*, 2300–2305.
38. European LeukemiaNet (2014). Management of chronic myeloid leukemia (CML): recommendations from the European LeukemiaNet (ELN). http://www.leukemia-net.org/content/leukemias/cml/recommendations/index_eng.html
39. Baccarani, M., Castagnetti, F., Gugliotta, G., and Rosti, G. (2015). A review of the European LeukemiaNet recommendations for the management of CML. Ann. Hematol. *94* (*Suppl 2*), S141–S147.
40. Lee, P.C., and Meisel, D. (1982). Adsorption and surface-enhanced Raman of dyes on silver and gold sols. J. Phys. Chem. *86*, 3391–3395.
41. American Type Culture Collection (2017). https://www.lgcstandards-atcc.org
42. Leibnitz Institute DSMZ - German Collection of Microorganisms and Cell Cultures (2017). https://www.dsmz.de/
43. Livak, K.J., and Schmittgen, T.D. (2001). Analysis of relative gene expression data using real-time quantitative PCR and the $2^{(-\Delta\Delta C(T))}$ method. Methods *25*, 402–408.
44. Strober, W. (2001). Trypan blue exclusion test of cell viability. Curr. Protoc. Immunol. *111*, A3.B.1–A3.B.3.

45. Tipping, A.J., Mahon, F.X., Zafirides, G., Lagarde, V., Goldman, J.M., and Melo, J.V. (2002). Drug responses of imatinib mesylate-resistant cells: synergism of imatinib with other chemotherapeutic drugs. Leukemia *16*, 2349–2357.

46. Silva, A., Luís, D., Santos, S., Silva, J., Mendo, A.S., Coito, L., Silva, T.F., da Silva, M.F., Martins, L.M., Pombeiro, A.J., et al. (2013). Biological characterization of the antiproliferative potential of Co(II) and Sn(IV) coordination compounds in human cancer cell lines: a comparative proteomic approach. Drug Metabol. Drug Interact. *28*, 167–176.

47. Sutradhar, M., Fernandes, A.R., Silva, J., Mahmudov, K.T., Guedes da Silva, M.F., and Pombeiro, A.J.L. (2016). Water soluble heterometallic potassium-dioxidovanadium(V) complexes as potential antiproliferative agents. J. Inorg. Biochem. *155*, 17–25.

48. Luís, D.V., Silva, J., Tomaz, A.I., de Almeida, R.F., Larguinho, M., Baptista, P.V., Martins, L.M., Silva, T.F., Borralho, P.M., Rodrigues, C.M., et al. (2014). Insights into the mechanisms underlying the antiproliferative potential of a Co(II) coordination compound bearing 1,10-phenanthroline-5,6-dione: DNA and protein interaction studies. J. Biol. Inorg. Chem. *19*, 787–803.